論文 / 著書情報
Article / Book Information

Title	McKibben Muscle with Elastic Thread Embedded in Parallel Extending Range of Motion of Muscle-Driven Robots
Authors	Ryota Kobayashi, Shoma Tanaka, Hiroyuki Nabae, Gen Endo, Koichi Suzumori
Citation	IEEE Robotics and Automation Letters, Volume 10, Issue 3, Page 2534-2541
Pub. date	2025, 1
DOI	https://doi.org/10.1109/LRA.2025.3528662
Creative Commons	Information is in the article.

McKibben Muscle With Elastic Thread Embedded in Parallel Extending Range of Motion of Muscle-Driven Robots

Ryota Kobayashi, *Graduate Student Member, IEEE*, Shoma Tanaka, Hiroyuki Nabae, *Member, IEEE*, Gen Endo, *Member, IEEE*, and Koichi Suzumori, *Senior Member, IEEE*

***Abstract*—The McKibben muscle, widely employed in antagonistic drive robots, exhibits approximately 20% contraction under pneumatic pressure but lacks crucial passive extensibility. Previous attempts to achieve passive extensibility resulted in reduced overall contraction ratios due to the series connection of elongation and contraction sections. This study proposes a novel artificial muscle design that achieves extension through external force by arranging extensible and contractile components in parallel. The proposed design incorporates a composite thread consisting of an elastic thread and an inextensible thread connected in series, arranged parallel to a conventional McKibben muscle. This configuration yields an artificial muscle capable of approximately 16% contraction and over 40% extension under external force when relaxed. The simplicity of this design facilitates straightforward integration into robotic systems. To demonstrate the efficacy of the proposed artificial muscle, we applied it to a tensegrity robot, exemplifying an antagonistic drive system. This application showcases the potential of our design to enhance the performance and versatility of soft robotic systems.**

***Index Terms*—McKibben muscle, soft robot applications.**

I. Introduction

THE McKibben muscle is a pneumatic actuator [1], [2]. This actuator possesses a simple structure comprising a rubber tube encased in a braided sleeve. The braiding angle of the sleeve determines whether the muscle contracts or extends upon application of pneumatic pressure, as analytically described by Schulte's model [3]. The contracting type of McKibben muscle is more manageable and frequently employed in robotic development, capable of achieving approximately 20% contraction. Despite their low mass of only a few tens of grams per meter, these muscles can generate substantial forces ranging from tens to hundreds of Newtons when subjected to pneumatic pressure of approximately 0.5 MPa. By exploiting this advantageous force-to-weight ratio, McKibben muscles have been implemented in diverse robotic applications, including robotic arms [2], bipedal walking robots [4], quadruped robots [5], [6], and hopping robots [7].

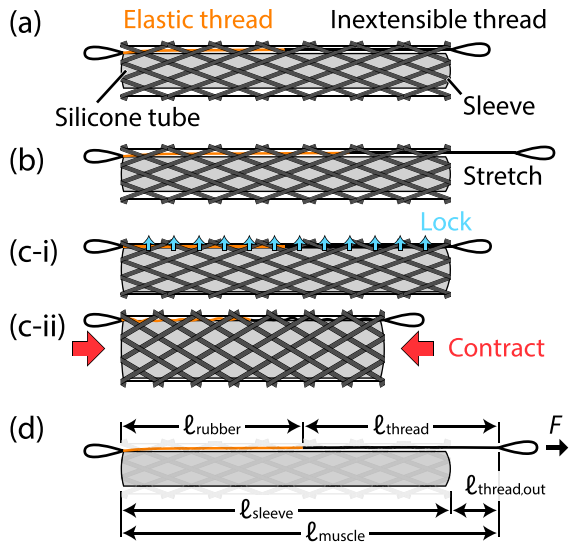

Fig. 1. (a) Structure of the proposed stretchable artificial muscle. (b) Extension of the artificial muscle is achieved by stretching the inner rubber thread. (c) Contraction mechanism: (c-i) Inner silicone tube presses the thread against the sleeve, locking it in place. (c-ii) Sleeve contraction pulling the locked thread, which buckles into a wavy pattern within the sleeve. (d) Internal structure and variables used in this letter, where $\ell_{\mathrm{thread,out}} = 0$ mm at $F = 0$ N.

The fundamental application of artificial muscles in these robotic systems involves antagonistic drive [2], [8], [9]. Antagonistic drive is a control methodology for manipulating the orientation of robotic arms and other components through the strategic arrangement of multiple contracting actuators that exert tensile forces in opposing directions. In this actuation paradigm, the contraction of one actuator induces passive extension in its counterpart. Consequently, an actuator lacking extensibility impedes the contractile function of its antagonistic pair. Therefore, these actuators must possess dual capabilities: active contraction from their initial length when driven and passive extension from their initial length under external forces when in a relaxed state. Critically, this extension functionality must remain dormant

Received 3 August 2024; accepted 27 December 2024. Date of publication 14 January 2025; date of current version 3 February 2025. This article was recommended for publication by Associate Editor Matteo Cianchetti and Editor Cecilia Laschi upon evaluation of the reviewers' comments. This work was supported in part by JSPS International Joint Research Program under Grant JPJSJRP20221502 and in part by JSPS KAKENHI under Grant JP24KJ1096. *(Corresponding author: Ryota Kobayashi.)*

The authors are with the Department of Mechanical Engineering, Institute of Science Tokyo, Meguro-ku 152-8550, Japan (e-mail: kobayashi.r.e4e3@m.isct.ac.jp).

This letter has supplementary downloadable material available at https://doi.org/10.1109/LRA.2025.3528662, provided by the authors.

Digital Object Identifier 10.1109/LRA.2025.3528662

during the contraction phase and should not affect the actuator's contractile performance.

McKibben muscles exhibit minimal extensibility under external forces due to the inherent constraints between the sleeve and rubber tube [10]. Consequently, when implementing antagonistic drive, artificial muscles are typically positioned with initial slack. This configuration precludes full utilization of their 20% contraction ratio. This reduction in the effective contraction ratio significantly constrains the development of McKibben muscle-based robots and limits their application scope.

To address this limitation due to contraction loss, a research study has investigated a braided artificial muscle that enables extension [11]. However, its extension ratio remains limited to 15% due to structural constraints. An alternative approach involves elastic elements in series with the artificial muscle, similar to Series Elastic Actuators (SEA). Yet, this configuration has contractile losses due to elastic deformation during muscle actuation, making modulating the elastic element stiffness desirable. In soft robotics, jamming mechanisms have been extensively studied for variable stiffness, with fiber jamming emerging as a technique for modulating tensile stiffness [12]. Pressure-based jamming systems have demonstrated superior stiffness modulation capabilities compared to vacuum-based approaches [13], [14]. By exploiting these principles, pressure-activated jamming mechanisms have shown effective passive extension in artificial muscles [15], [16]. Nevertheless, this approach faces critical limitations: the overall contraction ratio relative to the total length decreases with increasing extension segment length, as the extension segment provides only jamming functionality without the ability to contract. The complex structural design also introduces challenges such as response time limitations and fabrication complexity.

This study introduces a novel artificial muscle design based on the McKibben muscle, engineered to facilitate extension under external forces when relaxed. We achieved a new iteration of the McKibben muscle for the antagonistic drive only by adding a composite thread comprising of an elastic thread and an inextensible thread in series, arranged parallel to the conventional McKibben muscle configuration (Fig. 1). Through a single pressure input, the silicone tube compresses the thread against the sleeve, inducing pressure-driven jamming that simultaneously locks extension and enables contraction. In other words, the system exhibits stiffness variation like conventional jamming mechanisms and, moreover, functions as an actuator through its contractile capability. This design simplicity enhances its potential for robotic applications. To demonstrate the efficacy of this artificial muscle, we implement it in a tensegrity robot, which is conceptualized as an antagonistic drive system [17]. We achieved the large contractile deformation of tensegrity structures described in [18], [19] with a more straightforward configuration by utilizing artificial muscles with passive elongation capabilities.

The remainder of this letter is organized as follows: Section II proposes the structure and fabrication methodology of the proposed artificial muscle. Section III evaluates its characteristics, and Section IV discusses its application to tensegrity robots.

II. Artificial Muscle With Passive Elongation and Tension Generation for Antagonistic Drive

A. Structure of Proposed Artificial Muscle

Fig. 1 shows the proposed stretchable artificial muscle structure. This actuator integrates a composite thread comprising an elastic thread connected in series with an inextensible thread between the inner silicone tube and the sleeve of a McKibben muscle. The elastic thread's left end is fixed to the corresponding end of the inner silicone tube (Fig. 1(a)). The sleeve is secured at both ends to the silicone tube, preventing any slippage between the sleeve and the silicone tube. The variables used in this letter are defined in Fig. 1(d).

In the absence of pneumatic pressure, the actuator extends when the thread is pulled from the right side, owing to the thread's elasticity (Fig. 1(b)). Upon pneumatic pressurization, the silicone tube expands, causing sleeve contraction. This process locks the composite thread against the sleeve (Fig. 1(c-i)), followed by artificial muscle contraction due to sleeve constraints (Fig. 1(c-ii)). Consequently, the actuator behaves like a conventional McKibben muscle under pneumatic pressure while functioning as an elastic element in its unpressurized state. As the actuator contracts after locking the thread, this thread undergoes buckling within the sleeve.

Although a symmetric configuration can be realized by implementing dual threads on the upper and lower sides of the silicone tube, preliminary prototypes demonstrated that such configuration resulted in internal thread entanglement, impairing the extension mechanism. Hence, from a practical perspective, this study employs a single-thread configuration.

B. Fabrication Method of Proposed Artificial Muscle

Fig. 2 shows the fabrication process for the proposed artificial muscle. This process is adapted from the McKibben muscle's fabrication method described in [20]. This description details the production of a 200 mm artificial muscle. Initially, a pneumatic fitting (8.4 mm outer diameter) is inserted into a 200 mm tube (10 mm outer diameter, 8 mm inner diameter) and secured with adhesive (LOCTITE401, Henkel AG & Co. KGaA) (Fig. 2(a)). A rubber thread (3 mm outer diameter), an inextensible thread (0.75 mm outer diameter), and a silicone tube are attached using hose clamps to prevent air leakage. The rubber thread's knot is fixed to the left hose clamp. The rubber thread and inextensible threads are bonded, as shown in Fig. 2(b). The rubber thread end is frayed, adhesive is applied, and wrapped around the inextensible thread (Fig. 2(b-i, ii)). The rubber thread length is set to 50 mm.

The sleeve and silicone tube are secured together using hose clamps. Here, the 220 mm sleeve is used. The sleeve requires specific shaping (Fig. 2(c-iii)) to accommodate thread sliding at the hose clamp on the right side. Approximately 15 mm of the sleeve is initially hardened with adhesive to prevent fiber unraveling (Fig. 2(c-i)). Two 8 mm outer diameter pneumatic tubes are inserted during adhesive curing to maintain crosssectional integrity (Fig. 2(c-ii)). After the adhesive has dried, the sleeve is cut to the shape shown in Fig. 2(c-iii). As illustrated in Fig. 2(d),

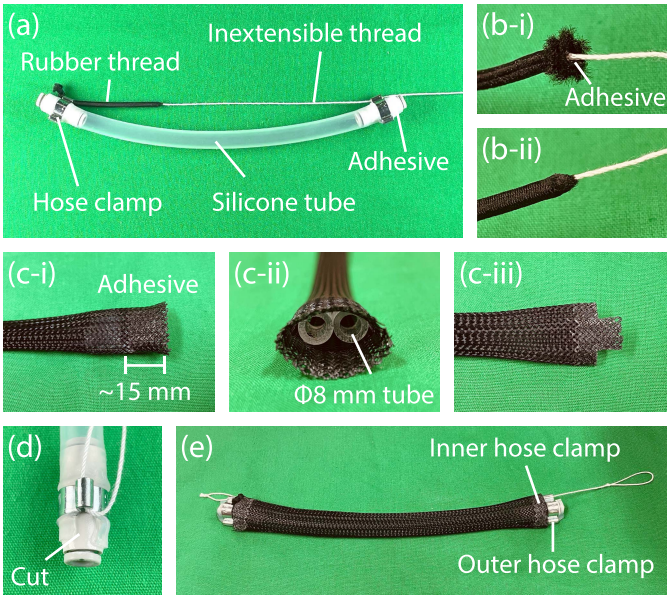

Fig. 2. Fabrication of stretchable muscle. (a) Internal structure assembly. (b) Connection between rubber thread and inextensible thread. (c) Sleeve preparation. (d) Cutting of silicone tube. (e) Sleeve installation.

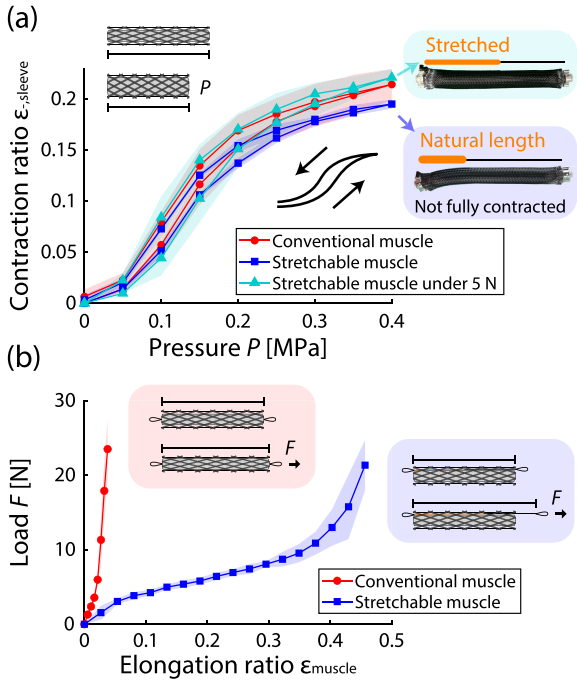

Fig. 3. Performance evaluation of conventional and stretchable artificial muscles. The plots display the mean values with shaded regions representing standard deviation (sample size = 5). (a) Sleeve contraction ratio as a function of applied pressure, without sleeve-thread slippage effects. The stretchable muscle achieves typical contraction ratios under load but shows a 2% lower ratio when unloaded, as the rubber thread cannot contract. (b) Load as a function of elongation ratio under unpressurized conditions.

the silicone tube is cut to prevent its entry into the hose clamp loop, thus minimizing thread friction. Then, the silicone tube, rubber thread, and inextensible thread are threaded through the sleeve and secured with hose clamps on both sides. As illustrated in Fig. 2(c-ii), the sleeve exhibits a slightly flattened circular cross-section, where the thread is positioned in the gap between the silicone tube and the sleeve (see Fig. 5(a-i) for reference).

III. Performance Evaluation of Proposed Artificial Muscles

A. Actuation Performance of Proposed Artificial Muscle

Fig. 3 illustrates the performance characteristics of the proposed artificial muscle and a conventional counterpart. The conventional artificial muscle specimen utilized identical dimensions: a 200 mm silicone tube and a 220 mm sleeve. Measurements were taken from five specimens, and the average and standard deviation values were used.

Fig. 3(a) depicts the contraction ratio of both artificial muscles concerning the pressure measured between the outer hose clamps. The contraction ratio $\varepsilon_{-,\mathrm{sleeve}}$ is expressed as follows:

$$\varepsilon_{-,\mathrm{sleeve}} = \frac{\ell_{\mathrm{sleeve},0} - \ell_{\mathrm{sleeve},P}}{\ell_{\mathrm{sleeve},0}}. \tag{1}$$

The parameters $\ell_{\mathrm{sleeve},0}$ and $\ell_{\mathrm{sleeve},P}$ denote the sleeve length ℓ_{sleeve} before pressurization and under pneumatic pressure P, respectively (Fig. 1(d)). The proposed artificial muscle under no load exhibits a contraction performance approximately 2% lower than conventional muscle while exhibiting a performance similar to that of conventional muscles under a 5 N load. This behavior can be attributed to the internal rubber thread being at its natural length in the unloaded state, making it difficult to achieve further contraction. The elastic force of the thread extends the sleeve from within, resulting in localized sleeve bending only in the region where the rubber thread is present, as observed in the lower image of Fig. 3(a). When an external load is applied, the rubber thread is pre-stretched before pressurization, enabling rubber thread contraction and preventing sleeve bending, as shown in the upper image of Fig. 3(a).

Fig. 3(b) illustrates the load-elongation ratio relationship for both artificial muscles. The elongation ratio $\varepsilon_{\mathrm{muscle}}$ is expressed as follows:

$$\varepsilon_{\mathrm{muscle}} = \frac{\ell_{\mathrm{muscle},F} - \ell_{\mathrm{muscle},0}}{\ell_{\mathrm{muscle},0}}, \tag{2}$$

where $\ell_{\mathrm{muscle},0}$ and $\ell_{\mathrm{muscle},F}$ represent the artificial muscle length ℓ_{muscle} without external force and under external force F, respectively (Fig. 1(d)). Measurements were conducted by fixing one end to a load cell and recording the load during extension. For the conventional artificial muscle, the length of sleeve ℓ_{sleeve} is equal to the length of muscle ℓ_{muscle} (Fig. 1(d)). Therefore the sleeve length was measured. These results demonstrate significantly improved extensibility under external forces in the proposed design. The extensional load characteristics can be readily modified by selecting appropriate internal rubber threads for specific applications. When higher elastic forces are required and the rubber thread diameter becomes excessive, additional rubber threads can be incorporated inside and outside the sleeve as auxiliary tensioners.

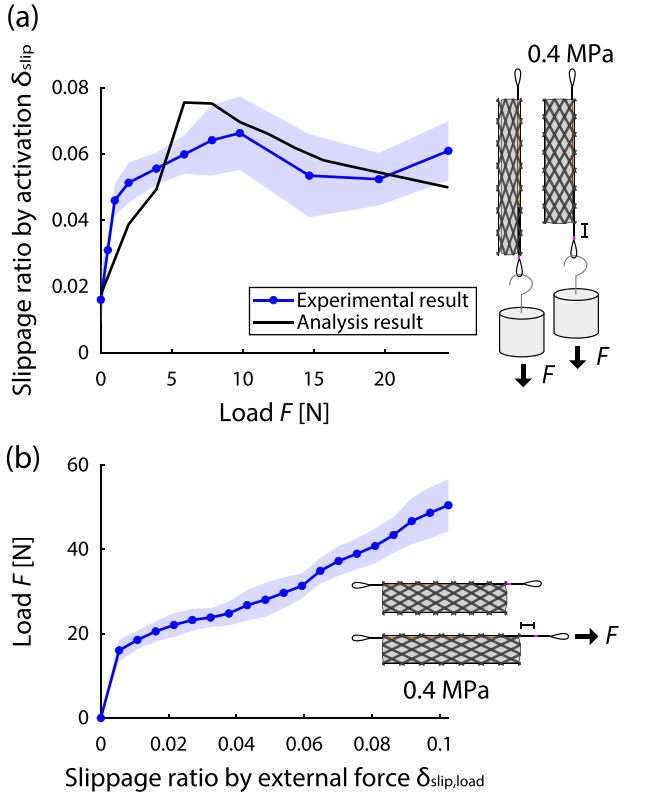

Fig. 4. Sleeve-thread slippage under different conditions. The plots display the mean values with shaded regions representing standard deviation (sample size = 5). (a) Slippage during pressurization to 0.4 MPa. (b) Force-induced slippage after applying 0.4 MPa.

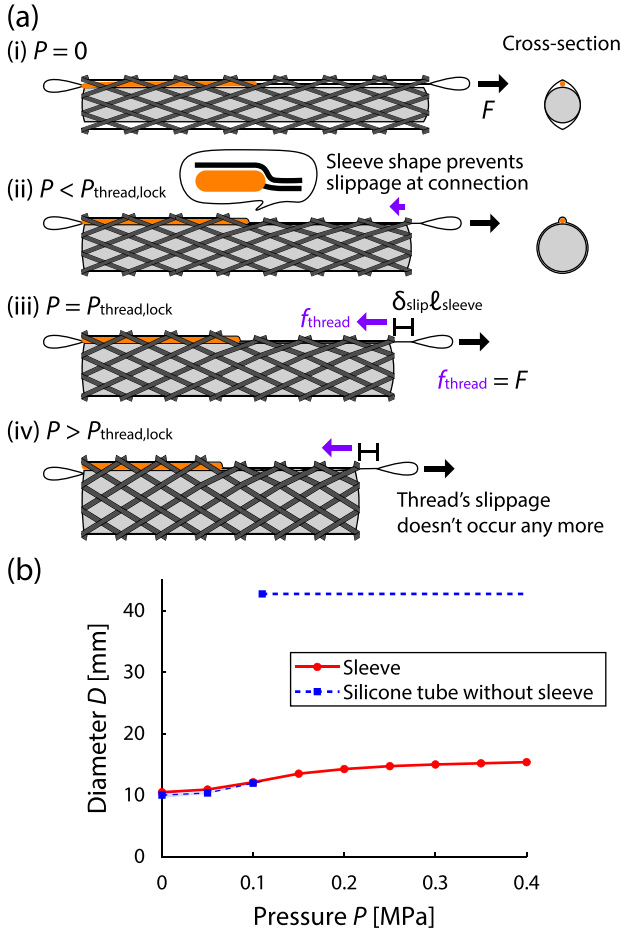

Fig. 5. (a) Detailed analysis of slippage mechanism from Fig. 1(a) to (c-ii). (b) Diameter of the sleeve and unconstrained silicone tube.

B. Slippage Between Sleeve and Thread of Proposed Artificial Muscle

Pressurization causes thread-sleeve slippage from Fig. 1(a) to (c-i), reducing the actuator's contraction length. Thus, the effective contraction ratio $\varepsilon_{-,\mathrm{muscle}}$ is expressed as follows:

$$\varepsilon_{-,\mathrm{muscle}} = \varepsilon_{-,\mathrm{sleeve}} - \delta_{\mathrm{slip}}, \tag{3}$$

where the slip ratio δ_{slip} is expressed as:

$$\delta_{\mathrm{slip}} = \frac{\ell_{\mathrm{thread,out},P} - \ell_{\mathrm{thread,out},0}}{\ell_{\mathrm{sleeve},0}}. \tag{4}$$

Here, $\ell_{\mathrm{thread,out},0}$ and $\ell_{\mathrm{thread,out},P}$ denote $\ell_{\mathrm{thread,out}}$ before pressurization and under pneumatic pressure P, respectively (Fig. 1(d)). Fig. 4 shows the slippage characteristics, with each data point representing the mean and standard deviation of five independent measurements.

Fig. 4(a) depicts the load-dependent slippage between the sleeve and thread. Measurements were conducted vertically with the artificial muscle oriented, subjected to constant loads via suspended weights, and pressurized at 0.4 MPa. Slippage increased with load up to approximately 10 N, plateauing around 6%. This results in an effective contraction of approximately 16% at 0.4 MPa and 5 N load (22% sleeve contraction minus 6% slippage). This actuator achieved passive stretchability under external force and active contraction ability, which is necessary for antagonistic drives.

Here, we discuss the slipping phenomenon between the thread and sleeve during pressurization. The thread-sleeve slipping phenomenon during pressurization is attributed to insufficient gripping force at low pressures. When applying 0.4 MPa, the internal pressure gradually rises from 0 MPa to 0.4 MPa. At lower pressures in this process, the frictional force remains insufficient to overcome the external load, preventing thread engagement. Once the pressure increases sufficiently, the sleeve locks the thread and initiates displacement with sleeve contraction. The slip magnitude corresponds to the sleeve contraction before thread displacement begins.

Experimental observations showed no slippage between the rubber thread and sleeve, which is explained by the mechanism in Fig. 5(a-ii). The design uses a rubber thread (3 mm diameter) and an inextensible thread (0.75 mm diameter). This diameter difference creates a sleeve step at their junction during silicone tube expansion, even at low pressures. During contraction, this step acts as a mechanical stop, synchronizing sleeve, and rubber thread movement. The junction experiences elastic and external forces from opposite sides, creating a differential force on the sleeve step. This force remained insufficient to overcome the junction step throughout testing, preventing rubber thread-sleeve slippage.

The pressure-dependent frictional force on the inextensible thread is hypothesized to be a function of sleeve diameter, silicone tube diameter, thread diameter, and applied pressure. Fig. 5(b) shows the silicone tube's pressure-diameter relationship without sleeve constraint, with significant expansion at 0.11 MPa and failure at higher pressures. The frictional force can be expressed as:

$$f_{\text{thread}}(P) = \mu\alpha(D_{\text{silicone}} + D_{\text{thread}} - D_{\text{sleeve}})P, \tag{5}$$

where α determines the normal force based on geometric parameters and pressure, μ represents the friction coefficient, and D_{silicone}, D_{thread}, and D_{sleeve} denote the diameters of the silicone tube, thread, and sleeve under pressure P, respectively. Due to the thread immediately becoming loose during sleeve contraction after locking, (5) considers force on a finite length at the thread's right end. For pressures above 0.11 MPa, the diameter at 0.11 MPa was used. The sleeve diameter is determined using the following [3]:

$$\frac{1}{\cos\theta_0} = \frac{1-\varepsilon_{-,\text{sleeve}}}{\cos\theta}, \quad \frac{\pi D_{\text{sleeve},0}}{\sin\theta_0} = \frac{\pi D_{\text{sleeve}}}{\sin\theta}, \tag{6}$$

where θ and θ_0 denote the sleeve's current and initial braiding angles, respectively, and $D_{\text{sleeve},0}$ represents the initial sleeve diameter. Defining $P_{\text{thread,lock}}$ as the pressure required for thread locking:

$$f_{\text{thread}}(P_{\text{thread,lock}}) = F. \tag{7}$$

Then, the thread section slip ratio is given by:

$$\delta_{\text{slip,thread}} = \varepsilon_{-,\text{sleeve}}(P_{\text{thread,lock}}), \tag{8}$$

where $\varepsilon_{-,\text{sleeve}}(P)$ represents the contraction ratio of the sleeve at applied pressure P. Considering that there is no slippage between the rubber thread and sleeve, the overall slip ratio is:

$$\delta_{\text{slip}} = \frac{\ell_{\text{sleeve},0} - \ell_{\text{rubber},0}}{\ell_{\text{sleeve},0}}\delta_{\text{slip,thread}}, \tag{9}$$

where $\ell_{\text{rubber},0}$ represents the initial length of the rubber thread.

The black line in Fig. 4(a) shows the analytical results using the proposed model, with $\mu\alpha$ in (5) set to 1 N/(MPa·mm). For a given load F, $P_{\text{thread,lock}}$ is determined using (5)-(7). Then, the thread section slip ratio is calculated using (8). The elastic thread length $\ell_{\text{rubber},0}$ under load F is obtained from Fig. 3(b), and the overall slip ratio is computed using (9), yielding the results shown in the figure. The analysis assumes a circular sleeve cross-section for simplicity despite its initially flattened geometry. Although higher loads increase the slip ratio $\delta_{\text{slip,thread}}$ in the inextensible thread section, the overall slip ratio remains stable due to the decreasing thread-to-sleeve length ratio described by (9). The discrepancies between analytical and experimental results can be attributed to unmodeled dynamic effects and nonlinear pressure-friction relationships.

Subsequently, the slip ratio $\delta_{\text{slip,load}}$ between the sleeve and thread, defined by the following equation, was experimentally evaluated under loading conditions after pressurization:

$$\delta_{\text{slip,load}} = \frac{\ell_{\text{thread,out},P,F} - \ell_{\text{thread,out},P}}{\ell_{\text{sleeve},0}}, \tag{10}$$

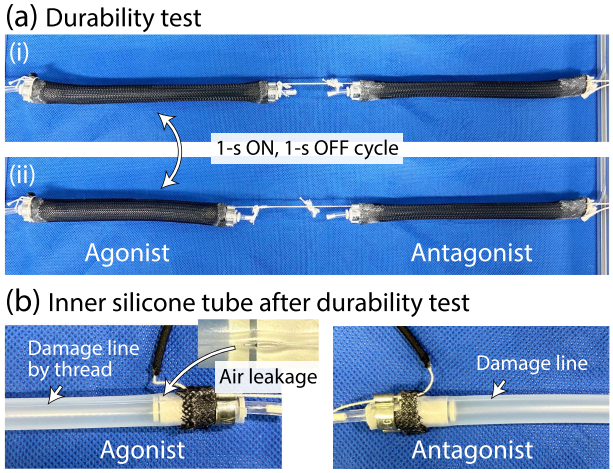

Fig. 6. (a) Durability test configuration: cyclic application of 0.3 MPa to agonist muscle. (b) Silicone tube damage after durability test.

where $\ell_{\text{thread,out},P,F}$ represents the exposed thread length $\ell_{\text{thread,out}}$ when a load is applied after pressurization. Fig. 4(b) illustrates the load-displacement characteristics of the proposed McKibben muscle under 0.4 MPa pneumatic pressure. Measurements were conducted with one end fixed to a load cell, recording values as both ends were pulled. An initial 5 N force was applied before pressurization. The thread exhibited minimal slippage until approximately 20 N of force was applied. As the sleeve contracts, the internal thread simultaneously becomes slack. When tension is applied to the thread, the slack is gradually eliminated, and the frictional force increases as the length of the tensioned thread section rises.

C. *Effects of Thread Integration on Artificial Muscle Durability*

Compared to conventional artificial muscles, the proposed design incorporates additional rubber thread and inextensible thread elements that create frictional contact with the silicone tube. Therefore, we conducted experimental evaluations to examine the effect of the internally integrated thread on the durability of the artificial muscle.

The experimental configuration is shown in Fig. 6(a). Durability testing was performed by serially connecting agonist and antagonist muscles and operating until agonist muscle failure. Due to the durability considerations of silicone tubes in artificial muscles, operation at 0.3 MPa is recommended. Accordingly, durability testing was conducted at this pressure level. The system was initialized by pre-stretching the internal rubber threads to maintain approximately 5 N tension on both threads in the unpressurized state. Cyclic pressurization (Fig. 6(a-ii)) and exhaustion (Fig. 6(a-i)) were performed at one-second intervals.

Five pairs of artificial muscles were subjected to durability testing. Among the agonist muscles tested, one specimen failed at 2,250 cycles due to silicone tube failure in a region independent of the added thread. In contrast, the remaining four specimens exhibited failure at a mean of 2,955 cycles (standard deviation: 838 cycles) due to thread-induced wear of the silicone

tube, as illustrated in Fig. 6(b). Similar wear patterns appeared in the antagonist muscles, though no such damage was observed in the rubber thread section.

While silicone tubes provide appropriate elasticity for McKibben muscles, their susceptibility to wear-induced failure poses significant durability challenges [21]. Consequently, implementing more wear-resistant elastomeric materials such as natural rubber or ethylene propylene diene monomer (EPDM) is recommended for applications requiring enhanced durability.

IV. Application of Proposed Artificial Muscles to a Tensegrity Robot With Antagonistic Drive

A. Tensegrity as an Antagonistic Driving System

To validate the proposed artificial muscle's applicability in antagonistic drive systems, we integrate it into a tensegrity structure. A tensegrity structure, comprising tension-bearing strings and compression-bearing struts, exemplifies an antagonistic drive system [17].

Implementing non-extensible artificial muscles as tensile members in tensegrity structures [22] results in rigid configurations that restrict large deformations. Our previous studies [18], [19] achieved large deformations by integrating artificially slackened artificial muscles. Although the reduction in contraction ratio caused by muscle slack was mitigated by routing the muscles through the strut elements, this configuration resulted in artificial muscles occupying the internal tensegrity volume, preventing effective space utilization. In this study, we demonstrate that the proposed extensible artificial muscles, when employed as tensile members, enable comparable large deformations characterized by axial compression and radial expansion without additional actuators, as previously achieved in [18], [19].

The tensegrity structure employed 400-mm-long stainless steel pipes as strut elements. For a significant deformation of the tensegrity, a 40 mm extension of the tension member is required in this case [18], [19]. The proposed artificial muscle can maintain tension in a straight configuration by shortening the rubber thread length to satisfy the following equation:

$$\ell_{\text{sleeve},0} - \ell_{\text{thread}} = \ell_{\text{rubber},0} > \ell_{\text{rubber,natural}}, \tag{11}$$

where $\ell_{\text{rubber},0}$ and $\ell_{\text{rubber,natural}}$ represent the rubber thread length in its straight, unpressurized state and its natural length, respectively. In this configuration, the artificial muscle is subjected to a tension force of

$$T = g(\ell_{\text{rubber},0} - \ell_{\text{rubber,natural}}), \tag{12}$$

where $g(\Delta\ell)$ denotes the load exerted on the rubber thread corresponding to elongation length $\Delta\ell$. Preliminary prototyping indicated that when using the rubber thread with characteristic shown in Fig. 3(b), a pre-stretching that induces approximately 5 N in each of the 24 tension members is necessary for stable posture maintenance. In addition, A shorter natural length of the rubber thread results in larger restoring forces during the tensegrity deformation due to increased force exerted on the thread. For this application, we determined the dimensions to achieve a relatively short natural length of the rubber thread

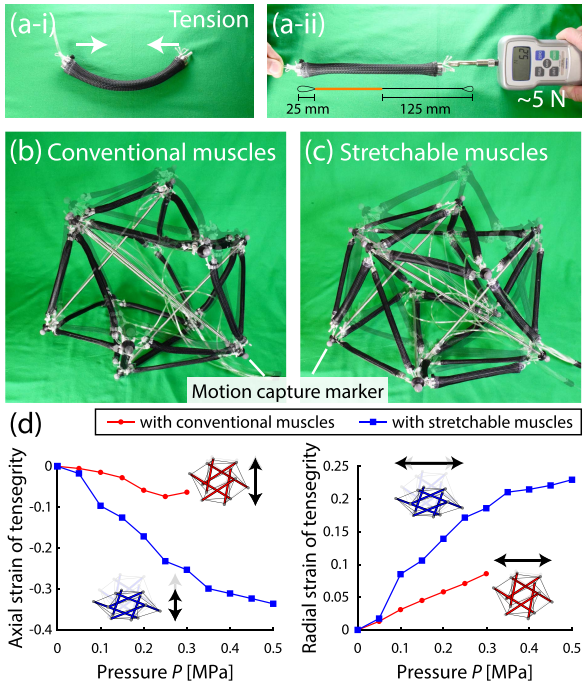

Fig. 7. (a) Stretchable artificial muscle generating 5 N tension at initial length. (b) , (c) Tensegrity deformation using conventional (b) and proposed artificial muscles (c). (d) Axial and radial strain versus applied pressure, where strain represents the length change indicated by arrows. Tensegrity visualization from motion capture data (red: with conventional McKibben muscles, blue: with proposed stretchable muscles).

while enabling approximately 40 mm extension under an initial tension of 5 N. Consequently, using the same silicone tube, sleeve, and rubber thread configuration as Section II-B, we constructed tensile members with modified thread lengths of 25 mm and 125 mm on the left and right sides, respectively, as shown in Fig. 7(a-ii).

Fig. 7(a) illustrates the manufactured stretchable McKibben muscle. The design leads to tension in the rubber thread when straightened, resulting in a bent state under no load, naturally curving toward the side with the rubber thread (Fig. 7(a-i)). When fully extended (Fig. 7(a-ii)), it generates approximately 5 N of tension.

B. Deformation of a Tensegrity Structure With Proposed Artificial Muscles

We construct tensegrity structures to evaluate the performance differential utilizing conventional artificial muscles and the proposed stretchable artificial muscles. The deformation characteristics of these structures are then comparatively analyzed.

For comparison, we constructed a tensegrity structure using conventional artificial muscles of the same length as our proposed stretchable artificial muscle (Fig. 7(b)). These conventional muscles were fixed in a slightly extended state to generate initial tension. Due to their limited extensibility under external forces, this configuration results in a comparatively rigid structure. Conversely, a tensegrity structure comprising 24

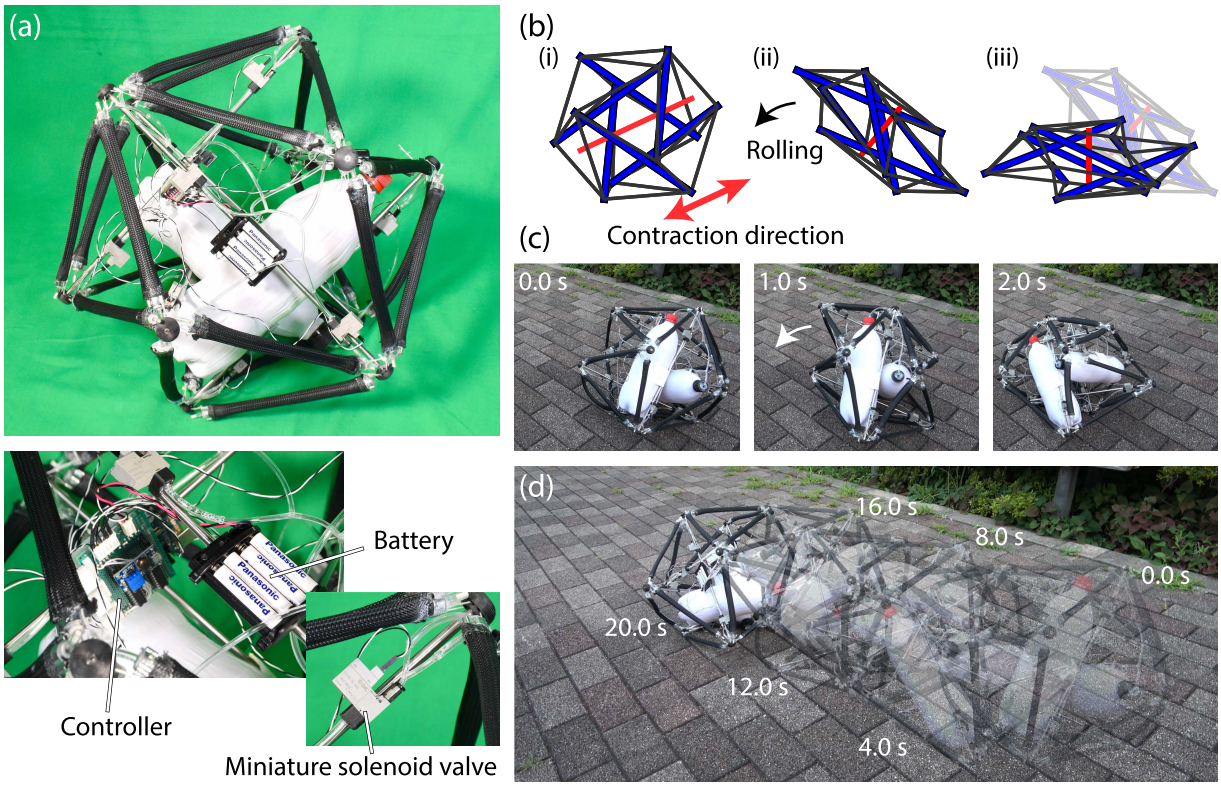

Fig. 8. (a) Untethered tensegrity robot equipped with solenoid valves, pneumatic tanks, a microcontroller, and batteries. (b) Rolling mechanism of the tensegrity robot utilizing large contraction deformation. (c) Experimental demonstration of the tensegrity robot's rolling motion. (d) Composite image of the tensegrity movement.

extensible artificial muscles proposed in this study (Fig. 7(c)) has flexibility.

Fig. 7(d) illustrate the axial and radial strains of the tensegrity structure when pneumatic pressure is applied to 12 artificial muscles. For a tensegrity with conventional artificial muscles, antagonism significantly impeded contraction, resulting in extreme tension and structural failure at 0.35 MPa. Consequently, data for a tensegrity with conventional muscles is presented up to 0.3 MPa. The proposed method achieved 4.0 times more considerable axial strain and 2.2 times more considerable radial strain in a tensegrity than conventional muscles. This performance enhancement confirms their efficacy in complex antagonistic drive systems.

C. Rolling Demonstration of the Tensegrity Robot With Proposed Artificial Muscle

While the tensegrity robot described in [18], [19] fills the internal space with artificial muscles, the stretchable artificial muscles eliminate the need for internal artificial muscles, freeing up space for the potential integration of pneumatic tanks, batteries, and control systems, thus enabling the achievement of untethered tensegrity modules. Such modules could potentially realize the inchworm robot [18] and manipulator [19]. For simplicity, this letter demonstrates the rolling motion of a tensegrity robot utilizing large contraction deformation.

We developed an integrated tensegrity robot incorporating miniature solenoid valves (SY113-5L-M3, SMC Co.), a pneumatic regulator, a microcontroller (Arduino Uno) for control, power supply (4 AAA batteries) for the microcontroller, and pneumatic tanks (two 1.5 L plastic bottles) within its structure. Fig. 8(a) illustrates the constructed tensegrity robot. The batteries, microcontroller, regulator, and pneumatic tanks are securely fixed to the struts. Twelve small solenoid valves are positioned at the strut ends, each controlling two artificial muscles. The contraction deformation shown in Fig. 7(c) is induced by activating six solenoid valves.

The rolling motion of the tensegrity is achieved through the contractile deformation. Fig. 8(b) illustrates the rolling process. Initially, contraction is initiated along an axis non-perpendicular to the ground, highlighted in red (Fig. 8(b-i)). The overall structural contraction facilitates a significant shift in the center of gravity (Fig. 8(b-ii)). This shift subsequently induces a rolling motion, aligning the contraction axis perpendicular to the ground (Fig. 8(b-iii)). By changing the contractile direction, the robot can roll to another direction.

Fig. 8(c) illustrates the rolling experiment. The pneumatic tank was initially pressurized to 0.9 MPa. The air pressure is regulated to approximately 0.5-0.6 MPa for operation using a regulator. This configuration enabled rolling motion where each roll cycle comprises a 2 s contraction and rolling phase initiated by pneumatic pressure application, followed by a 2 s return to the

original posture due to artificial muscle tension, totaling 4 s per roll. The robot can progress in three rolling directions, allowing zigzag pattern movement Fig. 8(d). Current limitations include the absence of an onboard pump and restricting movement to 5 rolls before gas depletion. However, integrating a small pump with 0.5 MPa output could enable long-distance locomotion.

The rolling motion enabled by the proposed artificial muscles exemplifies their capacity to expand the scope of robotic applications significantly.

V. Conclusion

This study proposes a novel, simple, extensible McKibben muscle designed for antagonistic drive applications. The proposed artificial muscle incorporates a minimalist modification to the conventional McKibben design, featuring only an additional composite thread (comprising a rubber thread and an inextensible thread) parallel to the muscle structure. This parallel configuration preserves the overall contraction ratio of the artificial muscle unaffected by the rubber thread section length.

We evaluated the sleeve's contraction ratio and the muscle's elongation capability. In addition, we examined the slippage between the sleeve and thread. The sleeve exhibited approximately 22% contraction at 0.4 MPa pressure and a 5 N load with 6% slippage. Notably, in the absence of pneumatic pressure, we observed passive elongation exceeding 40%. These results demonstrate the efficacy of the proposed design in achieving both significant contraction and extensive passive elongation, highlighting its potential for antagonistic drive systems.

Furthermore, we explored the application of the proposed artificial muscle in a tensegrity robot, which exemplify antagonistic drive systems. Incorporating 24 of these artificial muscles as tensile components in the tensegrity structure yielded significant deformation capabilities. We demonstrated a rolling motion selected for its simplicity of implementation.

Future work will focus on mitigating slippage during pneumatic pressure application and the durability of the actuator, aiming to enhance overall performance. This improvement is expected to significantly advance the capabilities of antagonistic drive robots utilizing artificial muscles, including robot arms, bipedal and quadrupedal locomotion systems, and tensegrity-based structures. Furthermore, this concept of passive extension through parallel elastic elements is not limited to McKibben muscles. Still, it can be applied to various non-extensible contractile artificial muscles such as Hydraulically Amplified Self-healing Electrostatic (HASEL) actuators. This advancement has the potential to broaden the utilization of artificial muscles across diverse robotic applications, opening new avenues for soft robotics research and development.

References

[1] H. Schulte, "The characteristics of the McKibben artificial muscle," *Appl. External Power Prosthetics Orthotics*, vol. 874, pp. 94–115, 1961.

[2] B. Tondu and P. Lopez, "Modeling and control of McKibben artificial muscle robot actuators," *IEEE Control Syst. Mag.*, vol. 20, no. 2, pp. 15–38, Apr. 2000, doi: 10.1109/37.833638.

[3] B. Tondu, "Modelling of the McKibben artificial muscle: A review," *J. Intell. Mater. Syst. Struct.*, vol. 23, no. 3, pp. 225–253, 2012, doi: 10.1177/1045389X11435435.

[4] K. Hosoda, T. Takuma, A. Nakamoto, and S. Hayashi, "Biped robot design powered by antagonistic pneumatic actuators for multi-modal locomotion," *Robot. Auton. Syst.*, vol. 56, no. 1, pp. 46–53, 2008, doi: 10.1016/j.robot.2007.09.010.

[5] H. Tanaka, T.-Y. Chen, and K. Hosoda, "Dynamic turning of a soft quadruped robot by changing phase difference," *Front. Robot. AI*, vol. 8, 2021, Art. no. 629523, doi: 10.3389/frobt.2021.629523.

[6] Y. Masuda, K. Miyashita, K. Yamagishi, M. Ishikawa, and K. Hosoda, "Brainless running: A quasi-quadruped robot with decentralized spinal reflexes by solely mechanical devices," in *Proc. IEEE/RSJ Int. Conf. Intell. Robots Syst.*, 2020, pp. 4020–4025, doi: 10.1109/IROS45743.2020.9340807.

[7] N. Delson, T. Hanak, K. Loewke, and D. N. Miller, "Modeling and implementation of McKibben actuators for a hopping robot," in *Proc. IEEE 12th Int. Conf. Adv. Robot.*, 2005, pp. 833–840, doi: 10.1109/ICAR.2005.1507504.

[8] B.-S. Kang, C. S. Kothera, B. K. S. Woods, and N. M. Wereley, "Dynamic modeling of McKibben pneumatic artificial muscles for antagonistic actuation," in *Proc. IEEE Int. Conf. Robot. Automat.*, 2009, pp. 182–187, doi: 10.1109/ROBOT.2009.5152280.

[9] X. Chen, W. Zhu, W. Liang, Y. Lang, and Q. Ren, "Control of antagonistic McKibben muscles via a bio-inspired approach," *J. Bionic Eng.*, vol. 19, no. 6, pp. 1771–1789, 2022, doi: 10.1007/s42235-022-00225-w.

[10] G. Klute, J. Czerniecki, and B. Hannaford, "McKibben artificial muscles: Pneumatic actuators with biomechanical intelligence," in *Proc. IEEE/ASME Int. Conf. Adv. Intell. Mechatron.*, 1999, pp. 221–226, doi: 10.1109/AIM.1999.803170.

[11] G. Na, H. Nabae, and K. Suzumori, "Braided thin McKibben muscles for musculoskeletal robots," *Sensors Actuators A: Phys.*, vol. 357, 2023, Art. no. 114381, doi: 10.1016/j.sna.2023.114381.

[12] B. Yang et al., "Reprogrammable soft actuation and shape-shifting via tensile jamming," *Sci. Adv.*, vol. 7, no. 40, 2021, Art. no. eabh2073, doi: 10.1126/sciadv.abh2073.

[13] I. Onda, M. Watanabe, K. Tadakuma, K. Abe, and S. Tadokoro, "Tube mechanism with 3-axis rotary joints structure to achieve variable stiffness using positive pressure," *IEEE Robot. Automat. Lett.*, vol. 9, no. 1, pp. 675–682, Jan. 2024, doi: 10.1109/LRA.2023.3234767.

[14] G. B. Crowley, X. Zeng, and H.-J. Su, "A 3D printed soft robotic gripper with a variable stiffness enabled by a novel positive pressure layer jamming technology," *IEEE Robot. Automat. Lett.*, vol. 7, no. 2, pp. 5477–5482, Apr. 2022, doi: 10.1109/LRA.2022.3157448.

[15] S. Tanaka, H. Nabae, and K. Suzumori, "Back-stretchable McKibben muscles: Expanding the range of antagonistic muscle driven joints," *IEEE Robot. Automat. Lett.*, vol. 8, no. 9, pp. 5331–5337, Sep. 2023, doi: 10.1109/LRA.2023.3293316.

[16] S. Tanaka, R. Kobayashi, H. Nabae, and K. Suzumori, "Fiber jamming mechanism for back-stretchable McKibben muscles," in *Proc. IEEE/SICE Int. Symp. Syst. Integr.*, 2024, pp. 48–53, doi: 10.1109/SII58957.2024.10417652.

[17] I.-W. Park and V. SunSpiral, "Impedance controlled twisted string actuators for tensegrity robots," in *Proc. IEEE 14th Int. Conf. Control, Automat. Syst.*, 2014, pp. 1331–1338, doi: 10.1109/ICCAS.2014.6987763.

[18] R. Kobayashi, H. Nabae, G. Endo, and K. Suzumori, "Soft tensegrity robot driven by thin artificial muscles for the exploration of unknown spatial configurations," *IEEE Robot. Automat. Lett.*, vol. 7, no. 2, pp. 5349–5356, Apr. 2022, doi: 10.1109/LRA.2022.3153700.

[19] R. Kobayashi, H. Nabae, and K. Suzumori, "Active-bending six-bar tensegrity modular robot driven by thin artificial muscles," *IEEE Robot. Automat. Lett.*, vol. 8, no. 11, pp. 7400–7407, Nov. 2023, doi: 10.1109/LRA.2023.3315537.

[20] K. Naniwa, Y. Masuda, D. Nakanishi, D. Ura, and S. Yasuhiro, "A musculoskeletal robot tool kit: Recipes for open source artificial muscles and experimental environments (in Japanese)," in *Proc. Proc. JSME Annu. Conf. Robot. Mechatron.*, 2022, pp. 2A2–M08, doi: 10.1299/jsmermd.2022.2A2-M08.

[21] G. Klute and B. Hannaford, "Fatigue characteristics of McKibben artificial muscle actuators," in *Proc. IEEE/RSJ Int. Conf. Intell. Robots Syst. Innov. Theory, Pract. Appl.*, 1998, pp. 1776–1781, doi: 10.1109/IROS.1998.724854.

[22] Y. Koizumi, M. Shibata, and S. Hirai, "Rolling tensegrity driven by pneumatic soft actuators," in *Proc. IEEE Int. Conf. Robot. Automat.*, 2012, pp. 1988–1993, doi: 10.1109/ICRA.2012.6224834.